The Open Neuroimaging Journal
DOI: 10.2174/0118744400379054250428094005, 2025, 18, e18744400379054
ISSN: 1874-4400

RESEARCH ARTICLE **OPEN ACCESS**

Characterizing Multivariate Regional Hubs for Schizophrenia Classification, Sex Differences, and Brain Age Estimation Using Explainable AI

Yuzheng Nie[1,2,#], Taslim Murad[1,#], Hui-Yuan Miao[1,*, #], Puskar Bhattarai[1], Deepa S. Thakuri[1,3] and Ganesh B. Chand[1,4,5,6,*]

[1]*Department of Radiology, Mallinckrodt Institute of Radiology, Washington University School of Medicine, St. Louis, MO, USA*
[2]*Institute for Informatics, Data Science and Biostatistics, Washington University School of Medicine, St. Louis, MO, USA*
[3]*University of Missouri, School of Medicine, Columbia, MO, USA*
[4]*Imaging Core, Knight Alzheimer Disease Research Center, Washington University School of Medicine, St. Louis, MO, USA*
[5]*Institute of Clinical and Translational Sciences, Washington University School of Medicine, St. Louis, MO, USA*
[6]*NeuroGenomics and Informatics Center, Washington University School of Medicine, St. Louis, MO, USA*

Abstract:

Purpose: This study aimed to investigate multivariate regional patterns for schizophrenia (SZ) classification, sex differences, and brain age by utilizing structural MRI, demographics, and explainable artificial intelligence (AI).

Methods: Various AI models were employed, and the outperforming model was identified for SZ classification, sex differences, and brain age predictions. For the SZ and sex classification tasks, support vector classifier (SVC), k-nearest neighbor (KNN), and deep learning neural network (DL) models were compared. In the case of regression-based brain age prediction, Lasso regression (LR), Ridge regression (RR), support vector regression (SVR), and DL models were compared. For each regression or classification task, the optimal model was further integrated with the Shapley additive explanations (SHAP), and significant multivariate brain regional patterns were identified.

Results: Our results demonstrated that the DL model outperformed other models in SZ classification, sex differences, and brain age predictions. We then integrated outperforming DL model with SHAP, and this integrated DL-SHAP model was used to identify the individualized multivariate regional patterns associated with each prediction. Using the DL-SHAP approach, we found that individuals with SZ had anatomical changes, particularly in the left pallidum, left posterior insula, left hippocampus, and left putamen regions, and such changes associated with SZ were different between female and male patients. Finally, we further applied the DL-SHAP method to brain age prediction and suggested important brain regions related to aging in health controls (HC) and SZ processes.

Conclusion: This study systematically utilized predictive modeling and novel explainable AI approaches and identified the complex multivariate brain regions involved with SZ classification, sex differences, and brain aging, thereby building a deeper understanding of neurobiological mechanisms involved in the disease, offering new insights into future SZ diagnosis and treatments, and laying the foundation for the development of precision medicine.

Keywords: Machine learning, Deep learning, Schizophrenia classification, Brain age prediction, Sex differences, Shapley additive explanations.

*Address correspondence to these authors at the Department of Radiology, Mallinckrodt Institute of Radiology, Washington University School of Medicine, St. Louis, MO, USA, Imaging Core, Knight Alzheimer Disease Research Center, Washington University School of Medicine, St. Louis, MO, USA, Institute of Clinical and Translational Sciences, Washington University School of Medicine, St. Louis, MO, USA and NeuroGenomics and Informatics Center, Washington University School of Medicine, St. Louis, MO, USA; E-mails: gchand@wustl.edu and miaoh@wustl.edu
#These authors contributed equally to this work

Cite as: Nie Y, Murad T, Miao H, Bhattarai P, Thakuri D, Chand G. Characterizing Multivariate Regional Hubs for Schizophrenia Classification, Sex Differences, and Brain Age Estimation Using Explainable AI. Open Neuroimaging J, 2025; 18: e18744400379054. http://dx.doi.org/10.2174/0118744400379054250428094005

Received: February 04, 2025
Revised: April 02, 2025
Accepted: April 02, 2025
Published: May 05, 2025

1. INTRODUCTION

Schizophrenia (SZ) is widely regarded as one of the most debilitating health conditions affecting humanity [1-6], with a lifetime prevalence of about 1% [7, 8]; it is known to affect 1 in 300 individuals [9]. Males and females are affected by the disease differently [10-12]. SZ causes severe behavioral dysfunctions, like hallucinations, delusions, and cognitive impairments, in individuals, and it can accelerate brain aging processes by introducing brain alterations [13-22]. In contrast to the significant personal and socioeconomic burden caused by SZ, it remains challenging to reach a comprehensive understanding [6]. Despite extensive research and clinical efforts, effective personalized treatment options for SZ are still lacking. Therefore, building a deeper understanding of SZ mechanisms, especially important multivariate brain regions associated with SZ, is crucial for improving diagnosis, developing more effective treatment strategies, and promoting precision medicine efforts.

Integrating magnetic resonance imaging (MRI) of the brain with machine learning/artificial intelligence (ML/AI) has dominated exploratory research lately [9, 15, 23-31] for SZ classification and age predictions. Existing studies have primarily focused on predictive modeling, but the underlying neurobiological regional patterns associated with such predictions are poorly understood yet. Prior research examining which brain regions are closely related to SZ has primarily used a univariate approach, neglecting the multivariate associations between regions. For example, a study [32] demonstrated a correlation between the left putamen volume and the delusion evaluation in SZ. However, evaluating the association between individual brain regions and SZ could be problematic, because this method ignored the influence of activities from other brain regions. Theoretically, putamen could have no impact on SZ, and/or the symptom could be due to alterations in other brain regions. Different brain regions work in a collaborative way and various regions have been implicated to be involved in SZ mechanisms [33-38]. Thus, it is critical to systematically investigate the associations between the brain regions and SZ mechanisms in a multivariate way, thereby uncovering the complex neurobiological mechanisms of this disorder. In this study, we proposed to evaluate the association between a brain region and SZ while accounting for the contributions of other regions. In this way, we can be more confident of the association identified between the target region and SZ progression.

This study sought to investigate the underlying multivariate regional patterns associated with neurobiological mechanisms, focusing on SZ *vs*. control classification, as well as male *vs*. female classification and brain age predictions in SZ using a large sample of MRI and demographic data. For this, we built various AI models for these predictions and integrated the outperforming model with the feature importance method to explain/interpret the predictions and identify the corresponding multivariate regional patterns. Since individuals with SZ have been reported to exhibit brain regional changes [23, 39-44], we hypothesized that our explainable AI approach can predict SZ *vs*. control classification and identify the multivariate regional contributors to such prediction. Since male *vs*. female disparity has been suggested in SZ [12, 45, 46], we hypothesized that our explainable AI-based modeling can characterize the neurostructural correlates in a multivariate fashion. Since some studies have suggested the effect of age on SZ [14, 47], we further tested this using our explainable AI approach. With the multivariate relationship between brain structure and SZ identified, our results could promote the understanding of the underlying mechanisms of SZ. Patients with obvious alterations in important brain hubs identified in our study should consider the risk of SZ and undergo further testing. In addition, a future direction of therapeutic intervention could be slowing down the alteration in the important brain hubs associated with SZ, as indicated by our results.

2. MATERIALS AND METHODS

2.1. Dataset

The dataset (N = 368, age: 18-66 years old; Table **1**) was obtained from Schizconnect [48, 49] (www.schizconnect.org), with centralization provided by the Center for Biomedical Research Excellence (COBRE) [50], Neuromorphometry by Computer Algorithm Chicago (NMorphCH) [51], and function Biomedical Informatics Research Network (fBIRN) PhaseII_0010 [52]. We only included participants categorized as SZ strict and healthy controls and for whom brain T1-weighted MR images and age and sex information were available. Out of 368 subjects, 165 (42 females) subjects belonged to the SZ group and 203 (79 females) were healthy controls (HC). We utilized the brain T1-weighted MR images and extracted brain volumes corresponding to 145 anatomical regions of interest (ROIs) using the multi-atlas region segmentation utilizing ense-

mbles of registration algorithms and parameters and locally optimal atlas selection (MUSE) [53]. These brain volumes were further corrected for the site and covariate effects using the harmonization technique [4, 54]. Using this harmonization approach, the sex and age effects were corrected for SZ classification, age effects were corrected for sex classification, and sex effects were corrected for brain age prediction. These harmonized brain regional volumes corresponding to 145 ROIs were utilized as inputs for the ML/DL models. The 145 ROIs included a wide range of tissue types, including gray matter, white matter, cerebrospinal fluid/ventricles, and brain stem.

Table 1. Demographic distribution of participants.

Dataset	Healthy Controls (HC)		Schizophrenia (SZ) Patients		Total
	Male	Female	Male	Female	
COBRE	67	27	61	14	169
NMorphCH	21	22	30	13	86
fBIRNPhase11	36	30	32	15	113
Total	124	79	123	42	368

2.2. SZ-related Classification and Regression Tasks and associated AI Models

We evaluated 3 SZ-related tasks, including two classification tasks and one regression task. The classification tasks included classifying SZ *vs*. HC and classifying male *vs*. female sex within the SZ group and HC group. We employed traditional ML models, including K-nearest neighbor (KNN) [36, 37] and support vector classifier (SVC) [38, 39], along with a deep learning neural networks (DL) model for classification tasks. The regression task estimated the brain age of SZ subjects. We employed traditional ML models, including Lasso regression (LR) [41, 42], Ridge regression (RR) [43, 44], and support vector regression (SVR) [55], as well as the DL model for the regression task.

The hyperparameters of traditional ML models were tuned with a grid search procedure, and the optimal hyperparameters were selected for each model and each classification or regression task. For KNN, the optimal number of neighbors was chosen from a range of 1-100 with an increment of 2. For SVC, the gamma value was chosen from -12 to -2 with an increment of 1. In addition, the Gaussian/radial basis function (RBF) kernel was employed, and we evaluated C values ranging from 0.2 to 2.6 with an increment of 0.2. For LR and RR, the optimal value for the alpha parameter was selected from the bounds 0.15-0.4 and 50-250, respectively. For SVR, an RBF kernel was employed, and the optimal values of gamma, epsilon, and c-values hyperparameters were selected from a range of -12 to -2 with an increment of 1, -7 to 3 with an increment of 1, and -5 to 4 with an increment of 1, respectively. To decide the optimal value, for each machine learning (ML) model, each hyperparameter was assigned a set of values, and all possible combinations were evaluated to identify the optimal configuration. The optimal performance was determined using the mean absolute error (MAE) loss function for the regression task and the log loss function for the classification task, with the lowest loss indicating the best-performing model.

We evaluated a DL model consisting of five dense hidden layers with a decreasing number of units in order of 200, 160, 120, 80, and 40 (Fig. **1**). Each dense layer was followed by a rectified linear unit (ReLU) activation function, a batch normalization layer, and a dropout layer with a 0.1 dropout rate to stabilize the model and accelerate the training process [56, 57]. The final output layer comprised a single-unit dense layer accompanied by a linear activation function for the regression task and a sigmoid activation function for the classification task. This architecture was chosen as it yielded the lowest loss (MAE loss for the regression task and BCE loss for the classification task) for both regression and classification tasks.

To ensure the robustness of our models, a 10-fold stratified cross-validation (CV) strategy was implemented for classification tasks, and a 10-fold cross-validation (CV) strategy was implemented for the regression task, where data were split into training and test sets. The training set was further divided into training and validation sets, where the validation set accounted for 10% of the original training set, to monitor the training loss during the CV-based iterative training. CV is critically acclaimed for enhancing model generalization, mitigating overfitting, and providing a more robust estimation of the model's performance on unseen data [58]. The outcomes reported here were obtained from the partitioned test set, which was not used in training the models. The traditional ML models were implemented in Python using the Python library Scikit-learn [59] and trained with the default settings. To train the DL model, the binary cross entropy (BCE) loss function was employed for classification, and the mean absolute error (MAE) loss function was utilized for regression tasks. After hyperparameter tuning, we selected 500 training epochs, 64 batch sizes, a 0.001 learning rate, and an ADAM optimizer. The results for the DL model were reported after running the model multiple times (*i.e.*, five times here) and averaging the results over runs for robustness purposes. For classification, a soft voting approach was employed to get averaged outputs. The DL model was implemented using Python libraries TensorFlow [60] and Keras [61].

Various AI models were compared for each classification or regression task and the outperforming model (*i.e.*, the DL model in our study) was integrated with the Shapley additive explanation (SHAP) [62], referred to as DL-SHAP model (Fig. **1**), to explain or interpret the model outputs, thereby identifying the significant multivariate regional contributions to each classification or regression task. SHAP approach was utilized in this study because it is a state-of-the-art strategy for the interpretability or explainability of complex models and it satisfies all three essential properties, particularly local accuracy, missingness, and consistency, which are critical for the interpretability or explainability and the accuracy of complex AI models. SHAP comprises model-specific approximations, integrates the strengths of all other additive feature attribution methods, and outperforms other methods.

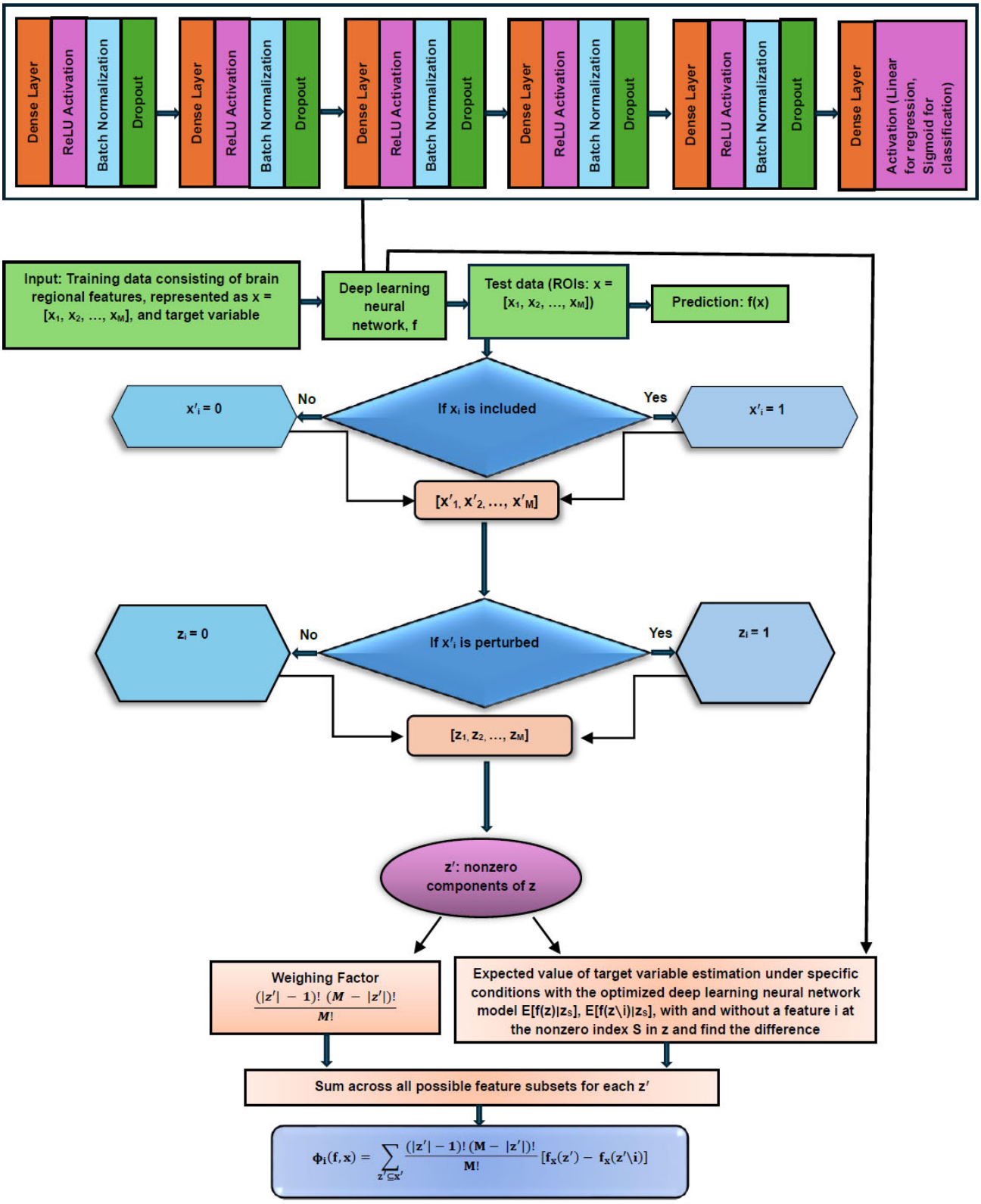

Fig. (1). Schematic diagram of DL-SHAP model.

This integration concept was originally proposed to investigate multivariate associations between brain regions and cognition in the context of Alzheimer's disease [63], and here, we intended to apply it to the schizophrenia domain. In DL-SHAP, the SHAP value for an input feature is computed by considering the contribution it makes to the final prediction of a participant. This contribution can be determined by observing the impact on the final output when the feature is added and when it is removed from the input. The SHAP value was calculated with the Python package SHAP. A higher absolute SHAP value indicates greater significance of the feature in obtaining the output. In our study, a higher absolute SHAP value associated with an ROI indicated a stronger association between that brain region and the related prediction of a participant. To aggregate the value across participants and evaluate the feature importance at the group level, we calculated the average absolute SHAP value over all participants, and regions with higher average absolute SHAP values over all participants within a group were believed to be important for the prediction results for that group of participants. It should be noted that the feature significance values with DL-SHAP across the models might vary as the contribution of the features to these models might change due to variations in architecture, weights, and the complexity of the model. Hence, the feature significance values with DL-SHAP are best used for understanding relative feature con-tributions within the same model, rather than for direct comparison across different models [62].

For assessing the classification model, we used micro-averaged accuracy, precision, recall, specificity, and F1-score as evaluation metrics. It is noteworthy that reporting multiple evaluation metrics can provide deeper insights into the models' performance. For regression tasks, we computed the Spearman correlation between the actual and predicted brain age, and the related *p*-values were estimated to evaluate the model's performance. Cohen's d-effect sizes were computed from DL-SHAP values to examine group differences. Group-wise DL-SHAP regional features and DL-SHAP group differences in terms of Cohen's d regional values were visualized using MRIcroGL [64]. Only ROIs with *p*-values less than 0.05, indicating statistical significance, were considered.

3. RESULTS

For the SZ *vs*. HC classification task, we found that the DL model outperformed (loss = 0.206, accuracy = 0.981, precision = 0.998, recall = 0.970, F1-score = 0.979, specificity = 0.990) all other traditional ML models in all evaluation metrics. The results of HC/SZ classification using various ML and DL models are listed in Table 2.

We then characterized the multivariate relationships between regional volumetric measures and HC/SZ classification using the DL-SHAP model. We identified the important brain regions for HC and SZ groups and their classification task. In the HC group, the top important regions were the left pallidum, left posterior insula, left hippocampus, fornix left, and left putamen, among others (Fig. 2a). In the SZ group, the top important regions identified were the left pallidum, left posterior insula, left hippocampus, right pallidum, and left putamen, among others (Fig. 2b). SHAP values at individual participant levels associated with the top important regions are visualized in Fig. (**S1**), which demonstrated the relationships between the volumetric measurements of individual ROI and SZ. For example, a larger pallidum was associated with a higher likelihood of being an SZ patient, and a smaller insula and hippocampus were associated with a higher likelihood of being an SZ patient. We then computed Cohen's d between HC and SZ groups using DL-SHAP regional features and found a few regions (Fig. 2c) that were not key hubs in each group.

Sex classification was performed within the HC group and the SZ group, respectively. Our results indicated that the DL model outperformed (SZ group: loss = 0.188, accuracy = 0.994, precision = 0.992, recall = 1, F1-score = 0.996, specificity = 0.976; HC group: loss = 0.162, accuracy = 0.995, precision = 1.000, recall = 0.992, F1-score = 0.996, specificity = 1.000) all other traditional ML models corresponding to all evaluation metrics. The results of sex classification using various ML and DL models are listed in Tables 3 and 4. We further investigated the multivariate relationships between regional volumetric measures and sex classification. The top important regions identified for males in the HC group were the left temporal pole, right posterior insula, left ventral DC, left hippocampus, and left entorhinal area (Fig. 3a); for males in the SZ group, the top important regions identified were the left posterior cingulate gyrus, left cuneus, right posterior orbital gyrus, left inferior temporal gyrus, and right inferior temporal gyrus (Fig. 3b); for females in the HC group, the top important regions identified were the left temporal pole, left ventral DC, left entorhinal area, right posterior insula, and right occipital lobe white matter (Fig. 3c); and for females in the SZ group, the top important regions identified were left posterior cingulate gyrus, corpus callosum, left inferior temporal gyrus, fourth ventricle, and right posterior orbital gyrus (Fig. 3d). We compared sex differences within each HC and SZ group with Cohen's d analysis (HC: Fig. 3e; SZ: Fig. 3f).

Table 2. SZ *vs*. HC classification. The test set performance of models. The optimal value for each evaluation metric is marked in bold. KNN: K-nearest neighborhood; SVC: Support vector classifier; DL: Deep learning neural networks.

Model	Accuracy	Precision	Recall	F1-score	Specificity	Loss
KNN	0.601	0.615	0.291	0.395	0.852	13.810
SVC	0.652	0.653	0.479	0.552	0.793	11.526
DL	**0.981**	**0.988**	**0.970**	**0.979**	**0.990**	**0.206**

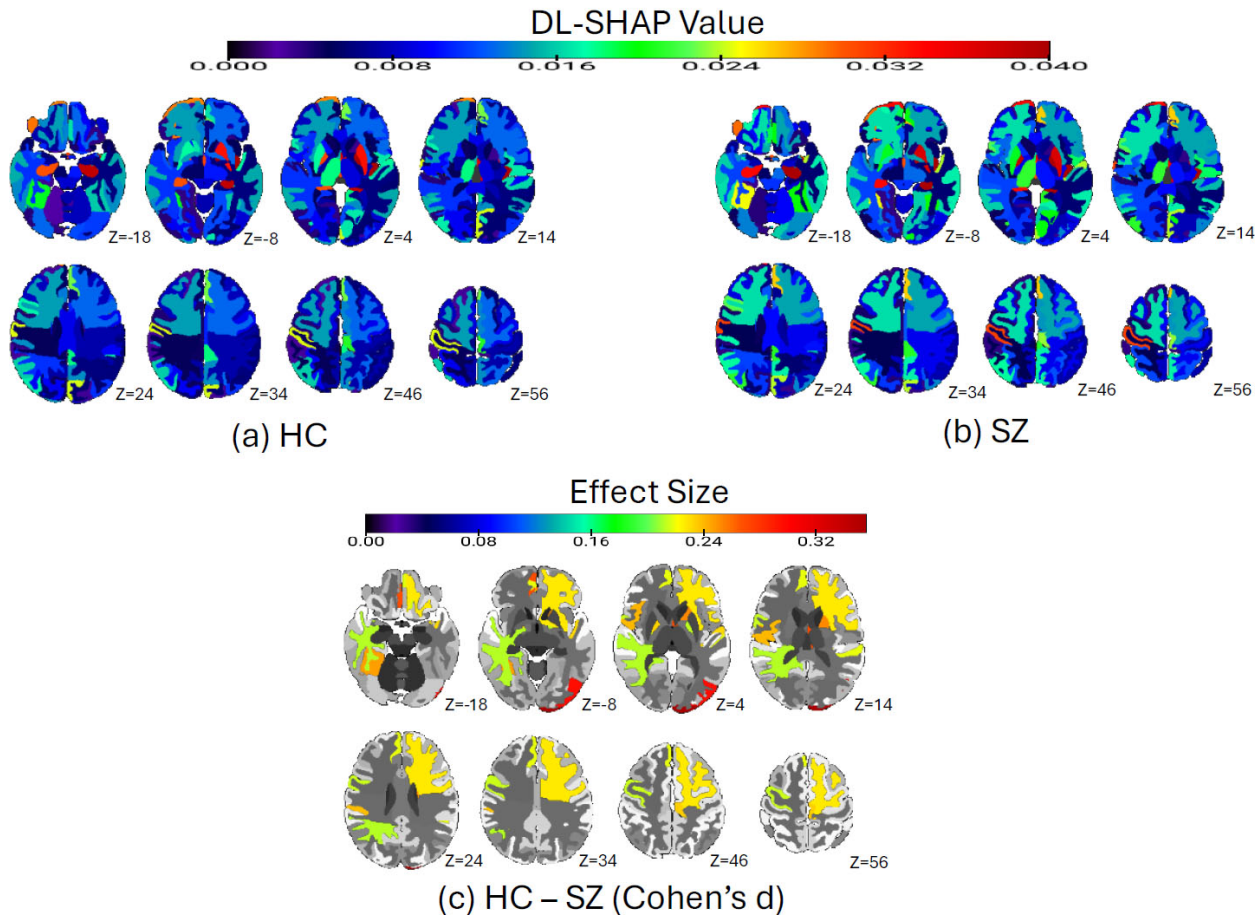

Fig. (2). SZ *vs*. HC diagnosis classification *via* DL-SHAP. (**a**) Significant brain regions in the HC group. The average absolute SHAP values of each brain region in the HC population are plotted. The color bar represents the average absolute SHAP value. (**b**) Significant brain regions in the SZ group. The average absolute SHAP values of each brain region in the HC population are plotted. The color bar represents the average absolute SHAP value. (**c**) The Cohen's d analysis comparing HC and SZ brains. We compared each ROI in HC and SZ brains by calculating the Cohen's d using the SHAP value of each participant in two populations, and the absolute effect size is plotted. The color bar represents the absolute value of effect size.

Table 3. Sex-wise classification within the SZ group. The test set performance of classification models. The optimal value for each evaluation is marked in bold.

Model	Accuracy	Precision	Recall	F1-score	Specificity	Loss
KNN	0.800	0.836	0.911	0.871	0.476	6.869
SVC	0.824	0.851	0.927	0.887	0.524	2.390
DL	**0.994**	**0.992**	**1.000**	**0.996**	**0.976**	**0.188**

Table 4. Sex-wise classification within the HC group. The test set performance of models. The optimal value for each evaluation metric is marked in bold.

Model	Accuracy	Precision	Recall	F1-score	Specificity	Loss
KNN	0.778	0.801	0.847	0.823	0.671	7.639
SVC	0.749	0.774	0.831	0.801	0.620	4.218
DL	**0.995**	**1.000**	**0.992**	**0.996**	**1.000**	**0.162**

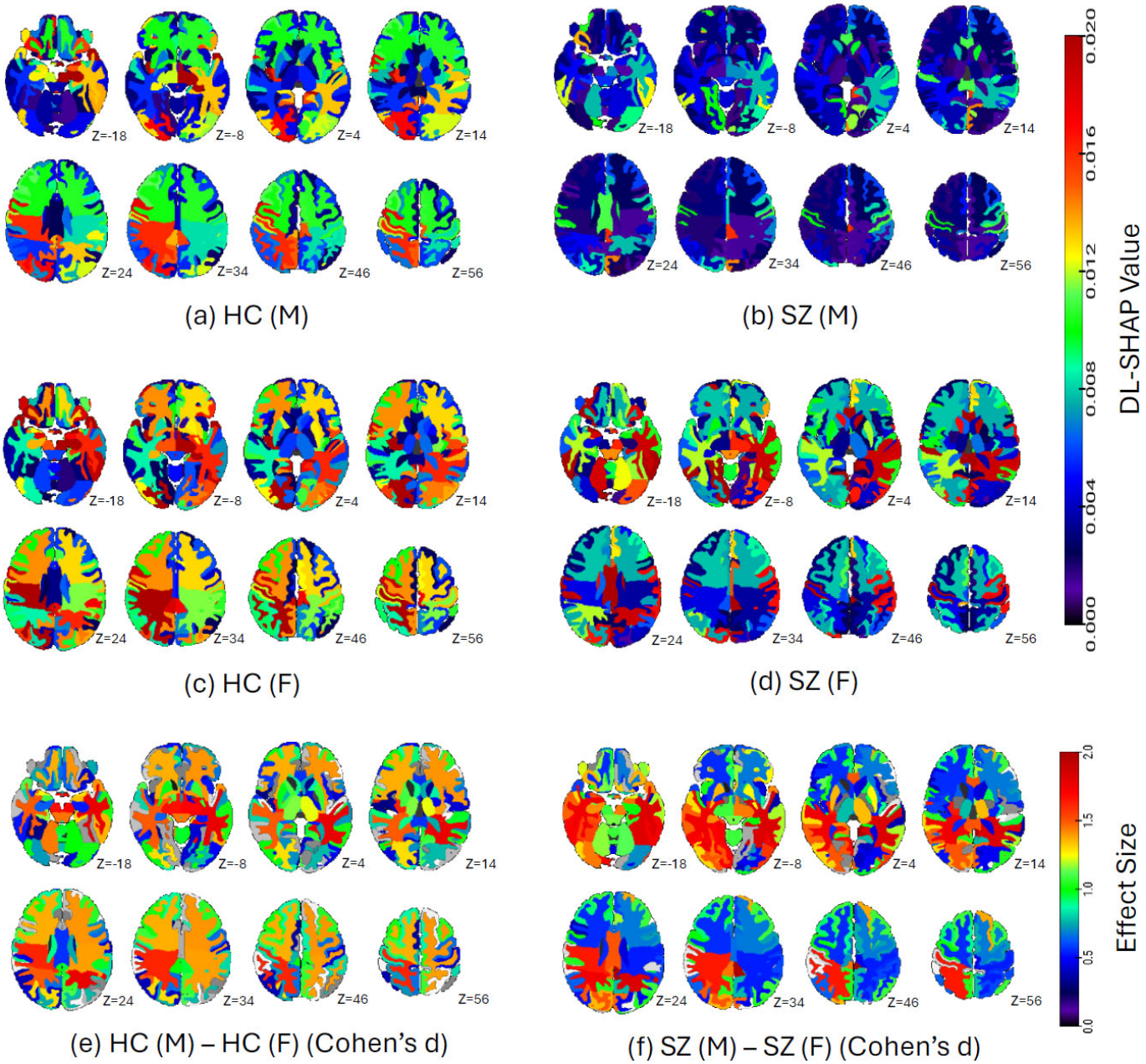

Fig. (3). Sex-wise classification within HC and SZ groups *via* DL-SHAP model. (**a**) Significant brain regions in males within the HC group for sex classification. The average absolute SHAP values of each brain region of male participants in the HC population are plotted. The color bar represents the average absolute SHAP value. (**b**) Significant brain regions in males for sex classification within the SZ group. The average absolute SHAP values of each brain region of male participants in the SZ population are plotted. The color bar represents the average absolute SHAP value. (**c**) Significant brain regions in females for sex classification within the HC group. The average absolute SHAP values of each brain region of female participants in the HC population are plotted. The color bar represents the average absolute SHAP value. (**d**) Significant brain regions in females within the SZ group. The average absolute SHAP values of each brain region of female participants in the SZ population are plotted. The color bar represents the average absolute SHAP value. (**e**) Cohen's d analysis (absolute value) comparing male and female brains in the HC group. We compared each ROI in male and female brains in the HC group by calculating Cohen's d using the SHAP value of each participant in two populations, and the absolute effect size is plotted. (**f**) Cohen's d analysis (absolute value) comparing male and female brains in the SZ group. We compared each ROI in male and female brains in the SZ group by calculating Cohen's d using the SHAP value of each participant in two populations, and the absolute effect size is plotted.

Finally, we found that the DL model outperformed all other traditional ML models in all evaluation metrics with a loss of 3.96 and a correlation of 0.92 (p = 7.9E-150) between the actual and predicted brain age (Fig. 4a). In contrast, the traditional ML models yielded a loss of around 7 and a correlation lower than 0.7. The results of brain age prediction using various ML and DL models are listed in Table 5. The multivariate relationships between the regional measures and brain age in SZ were also investigated using DL-SHAP. The top important regions identified for the HC group were the right superior frontal gyrus, left putamen, left supplementary motor cortex, right entorhinal area, and right subcallosal area, and the top important regions identified for the SZ group were the right superior frontal gyrus, left putamen, left pallidum, right subcallosal area, and right entorhinal area (Fig. 4b-d). Fig. (4b) shows the Cohen's d effect size differences between HC and SZ groups using DL-SHAP regional features.

Table 5. Brain age prediction. The test set performance of regression models in terms of MAE training loss, Spearman's correlation between actual and predicted brain age, and *p*-values. The optimal value for each evaluation metric is marked in bold. LR: Lasso regression; RR: Ridge regression; SVR: Support vector regression; DL: Deep learning neural networks.

Model	MAE Loss	Spearman's Correlation	*p*-value
LR	6.91	0.67	5.84E-49
RR	6.97	0.68	2.66E-50
SVR	7.53	0.60	1.03E-38
DL	**3.97**	**0.92**	**7.9E-150**

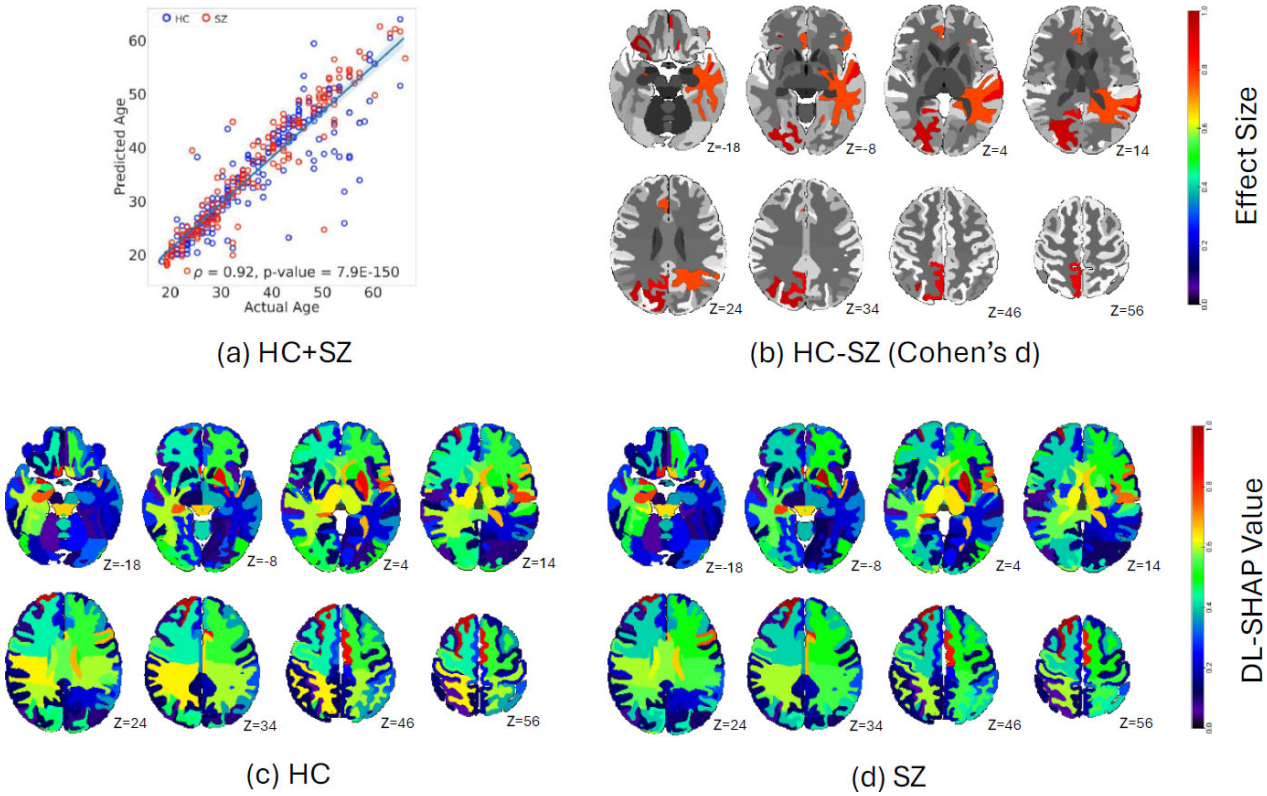

Fig. (4). Brain age prediction *via* the DL-SHAP model. (**a**) The correlation between actual and predicted brain age. (**b**) Cohen's d analysis (absolute value) comparing HC and SZ brains. We compared each ROI in HC and SZ brains by calculating Cohen's d using the SHAP value of each participant in two populations, and the absolute effect size is plotted. The color bar represents the absolute value of effect size. (**c**) The significant brain regions in the HC group. The average absolute SHAP values of each brain region in the HC population are plotted. The color bar represents the average absolute SHAP value. (**d**) The significant brain regions in the SZ group. The average absolute SHAP values of each brain region in the HC population are plotted. The color bar represents the average absolute SHAP value.

4. DISCUSSION

This study systematically investigated the hierarchy of multivariate brain regions associated with SZ mechanisms, particularly HC/SZ classification, sex classification, and brain age prediction. We found that the DL model outperformed the rest of the ML models in all classification- and regression-based predictions, and this finding was broadly consistent with previous studies [56, 57, 65-68] suggesting the superior performance of the DL model for classification and brain age predictions in various disorders, including SZ. This superior performance of the DL model might be due to being more complex compared to the rest of the ML models, such that it can capture the complex brain volumetric changes associated with HC/SZ, gender, and age. Such superior performance of DL was not limited to just SZ-related tasks, but it was found to be generalizable to different image modalities and diseases [69-73], suggesting the important role DL could play in future medical science development. The DL model proved to be a reliable model with decent performance for investigating the multivariate relationships between regional brain biomarkers and different aspects of SZ. We then integrated the outperforming DL model with SHAP, collectively referred to as DL-SHAP. The integrated DL-SHAP explainable AI approach uncovered the individuals with SZ to have anatomical changes, particularly in the left pallidum, left posterior insula, left hippocampus, and left putamen regions, and such brain alterations associated with SZ showed a different pattern in female and male patients.

We found important brain regions in terms of DL-SHAP regional features for HC and SZ classification tasks, suggesting that these regions undergo structural changes with the development of SZ. The identified key brain regions have been found to largely overlap with existing literature [74-79]. For example, subcortical structural abnormalities in SZ have been previously studied and the left pallidum and left putamen volumetric increases have been reported in SZ [76]. Our results have shown larger pallidum and putamen to be associated with a higher likelihood of being an SZ patient. The putamen alterations might contribute to the cognitive symptoms of SZ, such as auditory verbal hallucinations and cognitive dysfunction [80, 81]. The pallidum alterations might be related to the negative symptoms of SZ, given their role in reward and motivation [82]. The development of therapeutic treatments could consider slowing down or reverting the changes associated with those regions, which might reduce the SZ-related symptoms. Moreover, hippocampus and insula abnormalities have also been reported in SZ [77, 78]. Our results showed smaller insula and hippocampus to be associated with a higher likelihood of being an SZ patient. The broad agreement between our findings and the existing literature supports the validity of our results, but we innovatively identified the hierarchy of multivariate regions by considering their interactions using our novel DL-SHAP method for SZ *vs*. HC classification.

Previous studies have shown the susceptibility of males and females to SZ to be different [12, 45, 46]. We have extended these findings by examining sex differences in a fine-grained and multivariate regional manner. A general consensus in the field is that SZ is associated with reduced frontal and temporal volumes in males than females [46]. We identified the left inferior temporal gyrus and right posterior orbital gyrus to be important for sex classification in both male and female patients. In addition, similar to previous studies [83], we also identified the left posterior cingulate gyrus to be an important region for sex classification. Finally, ventricles and corpus callosum were shown to be different between male and female SZ patients [46]. In our study, they were identified as important regions for female SZ patients, but not as important for male SZ patients. While previous studies have shown that certain brain regions are affected differently in males and females with SZ, our study advanced this understanding by demonstrating that the importance of the same brain regions for sex classification varies between males and females, and that different brain regions contribute to sex classification in male and female SZ patients. These results and existing literature collectively suggest the complex interplay between sex and SZ, and such complex neurobiological regional patterns could be innovatively identified using our explainable AI approach in a multivariate way. The sex difference in SZ could arise from a combination of biological and environmental factors. For example, the hormonal difference, particularly the estrogen level in women, could play a role in sex differences in SZ [45]. In addition, environmental factors could also play a big role, as the cultural and social expectations are different for males and females, which could also shape brain structure development and alterations [84].

Finally, for brain age prediction, our findings regarding significant brain regions also overlapped with the existing literature. For instance, prior reports [47, 85] suggest that SZ has a strong impact on the aging process in the right superior frontal gyrus and putamen. While an increase in the volume of the entorhinal area was shown to be associated with SZ [86], it is new that our study explicitly demonstrated its aging process to be closely related to SZ. These findings and existing literature taken together suggested the impact of aging in HC and SZ processes. Brain age predictions could be used as a biomarker for SZ diagnosis. A study [15] showed SZ patients to deviate from the normal aging trajectory, as the predicted age was much higher than the actual chronological age. In reality, a quick computation of brain age and its deviation from the chronological age could be used as a risk factor for SZ.

One limitation of our study is that there are different subtypes of SZ [24, 87-91], but we could not investigate multivariate relationships between different brain regions and different subtypes due to the limitation of sample size. Future studies may consider employing a larger dataset, grouping participants by their SZ subtypes, and investigating the multivariate relationships between regional brain biomarkers and different SZ subtypes. Another limitation of our study was associated with the dataset. We observed that although significant efforts have been made to increase dataset sizes, an imbalance in the sex ratio persists. Given the sex difference in SZ, it would be important to consider including more female participants in the data collection plan in the future. Another limitation involved the unavailability of clinical variables, such as SZ symptoms, duration

of illness, and medication status, in this publicly available neuroimaging dataset. Thus, future studies should focus on examining those clinical measures in the context of the proposed explainable AI approaches and neuroimaging data. Also, this study focused on a single-session visit, not providing insights into how the multivariate relationships between brain structural alterations and SZ change with disease progression.

CONCLUSION

In conclusion, in this work, we utilized a range of ML/DL models to systematically investigate SZ neurobiological mechanisms, focusing on SZ classification, sex differences, and brain age using MRI and demographic data. The DL model outperformed other models in all classification and regression tasks. Our integrated novel DL-SHAP method further provided valuable insights into the dominant multivariate regional brain hubs associated with SZ diagnosis, sex-based differences, and brain age prediction. The findings collectively contributed to a deeper understanding of the underlying neurobiological mechanisms of SZ, offering new perspectives that could aid in diagnostic, prognostic, and therapeutic strategies.

Future studies should consider extending our results and evaluating how such multivariate relationships between brain alterations and SZ progression change over time and vary with different SZ subtypes, as well as studying clinical measures. Building a dataset with a more balanced sex ratio could also be an important goal for the entire field. This study is expected to serve as the foundation for extending these explainable AI approaches to other neuroimaging modalities, like fMRI, PET, EEG, *etc*., to achieve a multifactorial holistic understanding of SZ and other related disorders.

AUTHORS' CONTRIBUTIONS

It is hereby acknowledged that all authors have accepted responsibility for the manuscript's content and consented to its submission. They have meticulously reviewed all results and unanimously approved the final version of the manuscript.

LIST OF ABBREVIATIONS

SZ	=	Schizophrenia
AI	=	Artificial Intelligence
SVC	=	Support Vector Classifier
KNN	=	K-nearest Neighbor
DL	=	Deep Learning Neural Network
LR	=	Lasso Regression
RR	=	Ridge Regression
SVR	=	Support Vector Regression
SHAP	=	Shapley Additive Explanations
HC	=	Healthy Controls
ML	=	Machine Learning
MRI	=	Magnetic Resonance Imaging
MUSE	=	Multi-atlas region segmentation utilizing ensembles of registration algorithms and parameters and locally optimal atlas selection
ROIs	=	Regions of Interest
RBF	=	Radial Basis Function
ReLU	=	Rectified Linear Unit
CV	=	Cross-validation
BCE	=	Binary Cross Entropy
MAE	=	Mean Absolute Error

ETHICS APPROVAL AND CONSENT TO PARTICIPATE

Not applicable.

HUMAN AND ANIMAL RIGHTS

Not applicable.

CONSENT FOR PUBLICATION

Not applicable.

AVAILABILITY OF DATA AND MATERIALS

All data generated or analyzed during this study are included in this published article.

FUNDING

GBC is supported by the Mallinckrodt Institute of Radiology from Washington University in St. Louis as well as by the National Institutes of Health K01AG083230.

SchizConnect data collection and sharing for this project was funded by NIMH cooperative agreement 1U01 MH097435. COBRE data were downloaded from the Collaborative Informatics and Neuroimaging Suite Data Exchange tool (COINS; http://coins.mrn.org/dx) and data collection was performed at the Mind Research Network and funded by a Center of Biomedical Research Excellence (COBRE) grant 5P20RR021938/P20GM103472 from the NIH to Dr. Vince Calhoun. The fBIRN data used for this study were downloaded from the Function BIRN Data Repository (http://fbirnbdr.birncommunity.org:8080/BDR/), supported by grants to the Function BIRN (U24-RR021992) Testbed funded by the National Center for Research Resources at the National Institutes of Health, U.S.A. NMorhCH data used in the preparation of this article were obtained from the Neuromorphometry by Computer Algorithm Chicago (NMorphCH) dataset (http://nunda.northwestern.edu/nunda/data/projects/NMorphCH). As such, the investigators within NMorphCH contributed to the design and implementation of NMorphCH and/or provided data, but they did not participate in the analysis or writing of this report. Moreover, data collection and sharing for this project was funded by NIMH grant R01 MH056584.

CONFLICT OF INTEREST

Ganesh B Chand is the EIC of the journal TONIJ.

ACKNOWLEDGEMENTS

Declared none.

SUPPLEMENTARY MATERIAL

Supplementary material is available on the publisher's website along with the published article.

REFERENCES

[1] McCutcheon RA, Reis Marques T, Howes OD. Schizophrenia-an overview. JAMA Psychiatry 2020; 77(2): 201-10. PMID: 31664453

[2] Crespo-Facorro B, Such P, Nylander AG, *et al*. The burden of disease in early schizophrenia – A systematic literature review. Curr Med Res Opin 2021; 37(1): 109-21. http://dx.doi.org/10.1080/03007995.2020.1841618 PMID: 33095689

[3] Chand GB, Jiang H, Miller JP, Rhodes CH, Tu Z, Wong DF. Differential sphingosine-1-phosphate receptor-1 protein expression in the dorsolateral prefrontal cortex between schizophrenia type 1 and type 2. Front Psychiatry 2022; 13: 827981. http://dx.doi.org/10.3389/fpsyt.2022.827981 PMID: 35350429

[4] Chand GB, Singhal P, Dwyer DB, *et al*. Schizophrenia imaging signatures and their associations with cognition, psychopathology, and genetics in the general population. Am J Psychiatry 2022; 179(9): 650-60. http://dx.doi.org/10.1176/appi.ajp.21070686 PMID: 35410495

[5] Insel TR. Rethinking schizophrenia. Nature 2010; 468(7321): 187-93. http://dx.doi.org/10.1038/nature09552 PMID: 21068826

[6] Tandon R, Nasrallah H, Akbarian S, *et al*. The schizophrenia syndrome, circa 2024: What we know and how that informs its nature. Schizophr Res 2024; 264: 1-28. http://dx.doi.org/10.1016/j.schres.2023.11.015 PMID: 38086109

[7] Zhu C. Temporal dynamic synchronous functional brain network for schizophrenia classification and lateralization analysis. IEEE Trans Med Imaging 2024 Dec; 43(12): 4307-18. http://dx.doi.org/10.1109/TMI.2024.3419041

[8] Adamu MJ, Qiang L, Nyatega CO, *et al*. Unraveling the pathophysiology of schizophrenia: Insights from structural magnetic resonance imaging studies. Front Psychiatry 2023; 14: 1188603. http://dx.doi.org/10.3389/fpsyt.2023.1188603 PMID: 37275974

[9] Kanyal A, Mazumder B, Calhoun VD, *et al*. Multi-modal deep learning from imaging genomic data for schizophrenia classification. Front Psychiatry 2024; 15: 1384842. http://dx.doi.org/10.3389/fpsyt.2024.1384842 PMID: 39006822

[10] Galderisi S, Bucci P, Üçok A, Peuskens J. No gender differences in social outcome in patients suffering from schizophrenia. Eur Psychiatry 2012; 27(6): 406-8. http://dx.doi.org/10.1016/j.eurpsy.2011.01.011 PMID: 21616645

[11] Schultz SH, North SW, Shields CG. Schizophrenia: A review. Am Fam Physician 2007; 75(12): 1821-9. PMID: 17619525

[12] Salehi MA, Zafari R, Mohammadi S, *et al*. Brain-based sex differences in schizophrenia: A systematic review of fMRI studies. Hum Brain Mapp 2024; 45(5): e26664. http://dx.doi.org/10.1002/hbm.26664 PMID: 38520370

[13] Koutsouleris N, Davatzikos C, Borgwardt S, *et al*. Accelerated brain aging in schizophrenia and beyond: A neuroanatomical marker of psychiatric disorders. Schizophr Bull 2014; 40(5): 1140-53. http://dx.doi.org/10.1093/schbul/sbt142 PMID: 24126515

[14] Shahab S, Mulsant BH, Levesque ML, *et al*. Brain structure, cognition, and brain age in schizophrenia, bipolar disorder, and healthy controls. Neuropsychopharmacology 2019; 44(5): 898-906. http://dx.doi.org/10.1038/s41386-018-0298-z PMID: 30635616

[15] Bashyam VM, Erus G, Doshi J, *et al*. MRI signatures of brain age and disease over the lifespan based on a deep brain network and 14 468 individuals worldwide. Brain 2020; 143(7): 2312-24. http://dx.doi.org/10.1093/brain/awaa160 PMID: 32591831

[16] Shen CL, Tsai SJ, Lin CP, Yang AC. Progressive brain abnormalities in schizophrenia across different illness periods: A structural and functional MRI study. Schizophrenia 2023; 9(1): 2. http://dx.doi.org/10.1038/s41537-022-00328-7 PMID: 36604437

[17] DeLisi LE, Szulc KU, Bertisch HC, Majcher M, Brown K. Understanding structural brain changes in schizophrenia. Dialogues Clin Neurosci 2006; 8(1): 71-8. http://dx.doi.org/10.31887/DCNS.2006.8.1/ldelisi PMID: 16640116

[18] Shenton ME, Dickey CC, Frumin M, McCarley RW. A review of MRI findings in schizophrenia. Schizophr Res 2001; 49(1-2): 1-52. http://dx.doi.org/10.1016/S0920-9964(01)00163-3 PMID: 11343862

[19] Cheng Y, Cai H, Liu S, *et al*. Brain network localization of gray matter atrophy and neurocognitive and social cognitive dysfunction in schizophrenia. Biol Psychiatry 2025; 97(2): 148-56. http://dx.doi.org/10.1016/j.biopsych.2024.07.021 PMID: 39103010

[20] Xu R, Zhang X, Zhou S, *et al*. Brain structural damage networks at different stages of schizophrenia. Psychol Med 2024; 54(16): 4809-19. http://dx.doi.org/10.1017/S0033291724003088 PMID: 39660416

[21] McCutcheon RA, Keefe RSE, McGuire PK. Cognitive impairment in schizophrenia: Aetiology, pathophysiology, and treatment. Mol Psychiatry 2023; 28(5): 1902-18. http://dx.doi.org/10.1038/s41380-023-01949-9 PMID: 36690793

[22] Jiang S, Huang H, Zhou J, *et al*. Progressive trajectories of schizophrenia across symptoms, genes, and the brain. BMC Med 2023; 21(1): 237. http://dx.doi.org/10.1186/s12916-023-02935-2 PMID: 37400838

[23] Chand GB, Dwyer DB, Erus G, *et al*. Two distinct neuroanatomical subtypes of schizophrenia revealed using machine learning. Brain 2020; 143(3): 1027-38. http://dx.doi.org/10.1093/brain/awaa025 PMID: 32103250

[24] Chilla GS, Yeow LY, Chew QH, Sim K, Prakash KNB. Machine learning classification of schizophrenia patients and healthy controls using diverse neuroanatomical markers and Ensemble methods. Sci Rep 2022; 12(1): 2755. http://dx.doi.org/10.1038/s41598-022-06651-4 PMID: 35177708

[25] Zhang J, Rao VM, Tian Y, *et al*. Detecting schizophrenia with 3D structural brain MRI using deep learning. Sci Rep 2023; 13(1): 14433. http://dx.doi.org/10.1038/s41598-023-41359-z PMID: 37660217

[26] Priyanka G. Early diagnosis of schizophrenia in patients using deep learning techniques. 2024 10th International Conference on Advanced Computing and Communication Systems (ICACCS). 2024, pp. 809-815.

[27] Lee WH, Antoniades M, Schnack HG, Kahn RS, Frangou S. Brain age prediction in schizophrenia: Does the choice of machine learning algorithm matter? Psychiatry Res Neuroimaging 2021; 310: 111270. PMID: 33714090

[28] Kim WS, Heo DW, Maeng J, *et al*. Deep learning-based brain age prediction in patients with schizophrenia spectrum disorders. Schizophr Bull 2024; 50(4): 804-14. PMID: 38085061

[29] Haker R, Helft C, Natali Shamir E, *et al*. Characterization of brain abnormalities in lactational neurodevelopmental poly I:C rat model of schizophrenia and depression using machine-learning and quantitative MRI. J Magn Reson Imaging 2024. http://dx.doi.org/10.1002/jmri.29634 PMID: 39466009

[30] Di Camillo F, Grimaldi DA, Cattarinussi G, *et al*. Magnetic resonance imaging-based machine learning classification of schizophrenia spectrum disorders: A meta-analysis. Psychiatry Clin Neurosci 2024; 78(12): 732-43. http://dx.doi.org/10.1111/pcn.13736 PMID: 39290174

[31] Chatterjee I, Hilal B. Investigating the association between

symptoms and functional activity in brain regions in schizophrenia: A cross-sectional fmri-based neuroimaging study. Psychiatry Res Neuroimaging 2024; 344: 111870. PMID: 39142172

[32] Huang X, Pu W, Li X, *et al*. Decreased left putamen and thalamus volume correlates with delusions in first-episode schizophrenia patients. Front Psychiatry 2017; 8: 245. http://dx.doi.org/10.3389/fpsyt.2017.00245 PMID: 29209237

[33] Chand GB, Hajjar I, Qiu D. Disrupted interactions among the hippocampal, dorsal attention, and central-executive networks in amnestic mild cognitive impairment. Hum Brain Mapp 2018; 39(12): 4987-97. http://dx.doi.org/10.1002/hbm.24339 PMID: 30272830

[34] Chand GB, Thakuri DS, Soni B. Salience network anatomical and molecular markers are linked with cognitive dysfunction in mild cognitive impairment. J Neuroimaging 2022; 32(4): 728-34. http://dx.doi.org/10.1111/jon.12980 PMID: 35165968

[35] Chand GB, Wu J, Hajjar I, Qiu D. Interactions of the salience network and its subsystems with the default-mode and the central-executive networks in normal aging and mild cognitive impairment. Brain Connect 2017; 7(7): 401-12. http://dx.doi.org/10.1089/brain.2017.0509 PMID: 28707959

[36] Chand GB, Dhamala M. The salience network dynamics in perceptual decision-making. Neuroimage 2016; 134: 85-93. http://dx.doi.org/10.1016/j.neuroimage.2016.04.018 PMID: 27079535

[37] Chand GB, Dhamala M. Interactions between the anterior cingulate-insula network and the fronto-parietal network during perceptual decision-making. Neuroimage 2017; 152: 381-9. http://dx.doi.org/10.1016/j.neuroimage.2017.03.014 PMID: 28284798

[38] Thakuri DS, Bhattarai P, Wong DF, Chand GB. Dysregulated salience network control over default-mode and central-executive networks in schizophrenia revealed using stochastic dynamical causal modeling. Brain Connect 2024; 14(1): 70-9. http://dx.doi.org/10.1089/brain.2023.0054 PMID: 38164105

[39] Shenton ME, Whitford TJ, Kubicki M. Structural neuroimaging in schizophrenia from methods to insights to treatments. Dialogues Clin Neurosci 2010; 12(3): 317-32. http://dx.doi.org/10.31887/DCNS.2010.12.3/mshenton PMID: 20954428

[40] Haijma SV, Van Haren N, Cahn W, Koolschijn PCMP, Hulshoff Pol HE, Kahn RS. Brain volumes in schizophrenia: A meta-analysis in over 18 000 subjects. Schizophr Bull 2013; 39(5): 1129-38. http://dx.doi.org/10.1093/schbul/sbs118 PMID: 23042112

[41] Clementz BA, Sweeney JA, Hamm JP, *et al*. Identification of distinct psychosis biotypes using brain-based biomarkers. Am J Psychiatry 2016; 173(4): 373-84. http://dx.doi.org/10.1176/appi.ajp.2015.14091200 PMID: 26651391

[42] Gupta CN, Calhoun VD, Rachakonda S, *et al*. Patterns of gray matter abnormalities in schizophrenia based on an international mega-analysis. Schizophr Bull 2015; 41(5): 1133-42. http://dx.doi.org/10.1093/schbul/sbu177 PMID: 25548384

[43] Koutsouleris N, Gaser C, Jäger M, *et al*. Structural correlates of psychopathological symptom dimensions in schizophrenia: A voxel-based morphometric study. Neuroimage 2008; 39(4): 1600-12. http://dx.doi.org/10.1016/j.neuroimage.2007.10.029 PMID: 18054834

[44] Rozycki M, Satterthwaite TD, Koutsouleris N, *et al*. Multisite machine learning analysis provides a robust structural imaging signature of schizophrenia detectable across diverse patient populations and within individuals. Schizophr Bull 2018; 44(5): 1035-44. http://dx.doi.org/10.1093/schbul/sbx137 PMID: 29186619

[45] Li X, Zhou W, Yi Z. A glimpse of gender differences in schizophrenia. Gen Psychiatr 2022; 35(4): e100823. http://dx.doi.org/10.1136/gpsych-2022-100823 PMID: 36118418

[46] Mendrek A, Mancini-Marïe A. Sex/gender differences in the brain and cognition in schizophrenia. Neurosci Biobehav Rev 2016; 67: 57-78. http://dx.doi.org/10.1016/j.neubiorev.2015.10.013 PMID: 26743859

[47] Zhu J-D, Wu YF, Tsai SJ, Lin CP, Yang AC. Investigating brain aging trajectory deviations in different brain regions of individuals with schizophrenia using multimodal magnetic resonance imaging and brain-age prediction: A multicenter study. Transl Psychiatry 2023; 13(1): 82. http://dx.doi.org/10.1038/s41398-023-02379-5 PMID: 36882419

[48] Wang L. SchizConnect: Mediating neuroimaging databases on schizophrenia and related disorders for large-scale integration. Neuroimage 2016; 124(Pt B): 1155-67. http://dx.doi.org/10.1016/j.neuroimage.2015.06.065

[49] Ambite JL, Tallis M, Alpert K, *et al*. SchizConnect: Virtual data integration in neuroimaging. Data Integr Life Sci 2015; 9162: 37-51. http://dx.doi.org/10.1007/978-3-319-21843-4_4 PMID: 26688837

[50] Aine CJ, Bockholt HJ, Bustillo JR, *et al*. Multimodal neuroimaging in schizophrenia: Description and dissemination. Neuroinformatics 2017; 15(4): 343-64. http://dx.doi.org/10.1007/s12021-017-9338-9 PMID: 28812221

[51] Neuromorphometry by computer algorithm chicago (NMorphCH). Available from: http://nunda.northwestern.edu/nunda/data/projects/NMorphCH

[52] Keator DB. The function biomedical informatics research network data repository. Neuroimage 2016; 124(Pt B): 1074-9. http://dx.doi.org/10.1016/j.neuroimage.2015.09.003

[53] Doshi J, Erus G, Ou Y, *et al*. MUSE: MUlti-atlas region Segmentation utilizing Ensembles of registration algorithms and parameters, and locally optimal atlas selection. Neuroimage 2016; 127: 186-95. http://dx.doi.org/10.1016/j.neuroimage.2015.11.073 PMID: 26679328

[54] Fortin JP, Cullen N, Sheline YI, *et al*. Harmonization of cortical thickness measurements across scanners and sites. Neuroimage 2018; 167: 104-20. http://dx.doi.org/10.1016/j.neuroimage.2017.11.024 PMID: 29155184

[55] Chand GB, Habes M, Dolui S, Detre JA, Wolk DA, Davatzikos C. Estimating regional cerebral blood flow using resting-state functional MRI *via* machine learning. J Neurosci Methods 2020; 331: 108528. http://dx.doi.org/10.1016/j.jneumeth.2019.108528 PMID: 31756399

[56] Lam P. Accurate brain age prediction using recurrent slice-based networks. bioRxiv 2020.

[57] Kuo CY, Tai TM, Lee PL, *et al*. Improving individual brain age prediction using an ensemble deep learning framework. Front Psychiatry 2021; 12: 626677. http://dx.doi.org/10.3389/fpsyt.2021.626677 PMID: 33833699

[58] Kohavi R. A study of cross-validation and bootstrap for accuracy estimation and model selection. IJCAI'95: Proceedings of the 14th international joint conference on Artificial intelligence. Montreal, Quebec, Canada, 20 August 1995, pp. 1137 - 1143.

[59] Pedregosa F. Scikit-learn: Machine Learning in python. J Mach Learn Res 2011; 12: 2825-30.

[60] Abadi M. *TensorFlow: A system for large-scale machine learning*. USENIX Symposium on Operating Systems Design and Implementation. Savannah, GA, USA, 02 November 2016, pp. 265 - 283.

[61] Gulli A, Pal S. Deep learning with Keras. Packt Publishing Ltd. 2017.

[62] Lundberg SM, Lee S-I. *A unified approach to interpreting model predictions*. NIPS'17: Proceedings of the 31st International Conference on Neural Information Processing Systems. Long Beach, California, USA, 04 December 2017, pp. 4768 - 4777.

[63] Bhattarai P, Thakuri DS, Nie Y, Chand GB. Explainable AI-based deep-SHAP for mapping the multivariate relationships between regional neuroimaging biomarkers and cognition. Eur J Radiol

2024; 174: 111403.
http://dx.doi.org/10.1016/j.ejrad.2024.111403 PMID: 38452732
[64] MRIcroGL software. Available from: https://www.nitrc.org/projects/mricrogl
[65] Gong W, Beckmann CF, Vedaldi A, Smith SM, Peng H. Optimising a simple fully convolutional network for accurate brain age prediction in the PAC 2019 challenge. Front Psychiatry 2021; 12: 627996.
PMID: 34040552
[66] Oh J, Oh BL, Lee KU, Chae JH, Yun K. Identifying schizophrenia using structural MRI with a deep learning algorithm. Front Psychiatry 2020; 11: 16.
http://dx.doi.org/10.3389/fpsyt.2020.00016 PMID: 32116837
[67] Ahmedt-Aristizabal D, Fernando T, Denman S, *et al*. Identification of children at risk of schizophrenia *via* deep learning and EEG responses. IEEE J Biomed Health Inform 2021; 25(1): 69-76.
http://dx.doi.org/10.1109/JBHI.2020.2984238 PMID: 32310808
[68] Srinivasagopalan S, Barry J, Gurupur V, Thankachan S. A deep learning approach for diagnosing schizophrenic patients. J Exp Theor Artif Intell 2019; 31(6): 803-16.
http://dx.doi.org/10.1080/0952813X.2018.1563636
[69] Alhussen A, Anul Haq M, Ahmad Khan A, Mahendran RK, Kadry S. XAI-RACapsNet: Relevance aware capsule network-based breast cancer detection using mammography images *via* explainability O-net ROI segmentation. Expert Syst Appl 2025; 261: 125461.
http://dx.doi.org/10.1016/j.eswa.2024.125461
[70] Khan AA, Mahendran RK, Perumal K, Faheem M. Dual-3DM ^{3} AD: Mixed transformer based semantic segmentation and triplet pre-processing for early multi-class alzheimer's diagnosis. IEEE Trans Neural Syst Rehabil Eng 2024; 32: 696-707.
http://dx.doi.org/10.1109/TNSRE.2024.3357723 PMID: 38261494
[71] Kujur A, Raza Z, Khan AA, Wechtaisong C. Data complexity based evaluation of the model dependence of brain MRI images for classification of brain tumor and alzheimer's disease. IEEE Access 2022; 10: 112117-33.
http://dx.doi.org/10.1109/ACCESS.2022.3216393
[72] Khan AA, Madendran RK, Thirunavukkarasu U, Faheem M. *D*^{2}*PAM* : Epileptic seizures prediction using adversarial deep dual patch attention mechanism. CAAI Trans Intell Technol 2023; 8(3): 755-69.
http://dx.doi.org/10.1049/cit2.12261
[73] Perumal K, Mahendran RK, Ahmad Khan A, Kadry S. Tri-M2MT: Multi-modalities based effective acute bilirubin encephalopathy diagnosis through multi-transformer using neonatal Magnetic Resonance Imaging. CAAI Trans Intell Technol 2025; cit2.12409.
http://dx.doi.org/10.1049/cit2.12409
[74] Ito S, Miura K, Miyayama M, *et al*. Association between globus pallidus volume and positive symptoms in schizophrenia. Psychiatry Clin Neurosci 2022; 76(11): 602-3.
http://dx.doi.org/10.1111/pcn.13465 PMID: 36000224
[75] Yasuda Y, Okada N, Nemoto K, *et al*. Brain morphological and functional features in cognitive subgroups of schizophrenia. Psychiatry Clin Neurosci 2020; 74(3): 191-203.
http://dx.doi.org/10.1111/pcn.12963 PMID: 31793131
[76] Tang Y, Li Y, Cao P, *et al*. Striatum and globus pallidus structural abnormalities in schizophrenia: A retrospective study of the different stages of the disease. Prog Neuropsychopharmacol Biol Psychiatry 2024; 133: 111022.
http://dx.doi.org/10.1016/j.pnpbp.2024.111022 PMID: 38692473
[77] Wegrzyn D, Juckel G, Faissner A. Structural and functional deviations of the hippocampus in schizophrenia and schizophrenia animal models. Int J Mol Sci 2022; 23(10): 5482.
http://dx.doi.org/10.3390/ijms23105482 PMID: 35628292
[78] Sheffield JM, Rogers BP, Blackford JU, Heckers S, Woodward ND. Insula functional connectivity in schizophrenia. Schizophr Res 2020; 220: 69-77.
http://dx.doi.org/10.1016/j.schres.2020.03.068 PMID: 32307263
[79] Tohid H, Faizan M, Faizan U. Alterations of the occipital lobe in schizophrenia. Neurosciences 2015; 20(3): 213-24.
PMID: 26166588
[80] Gupta PK. Putamen inflammation and its association with working memory impairments in schizophrenia spectrum disorders. Biol Psychiatry 2020; 87(9): S213-4.
[81] Cui L-B, Liu K, Li C, *et al*. Putamen-related regional and network functional deficits in first-episode schizophrenia with auditory verbal hallucinations. Schizophr Res 2016; 173(1-2): 13-22.
http://dx.doi.org/10.1016/j.schres.2016.02.039 PMID: 26995674
[82] Schijven D, Postema MC, Fukunaga M, *et al*. Large-scale analysis of structural brain asymmetries in schizophrenia *via* the ENIGMA consortium. Proc Natl Acad Sci USA 2023; 120(14): e2213880120.
http://dx.doi.org/10.1073/pnas.2213880120 PMID: 36976765
[83] Lang X-E, Zhu D, Zhang G, *et al*. Sex difference in association of symptoms and white matter deficits in first-episode and drug-naive schizophrenia. Transl Psychiatry 2018; 8(1): 281.
http://dx.doi.org/10.1038/s41398-018-0346-9 PMID: 30563964
[84] Giordano GM, Bucci P, Mucci A, Pezzella P, Galderisi S. Gender differences in clinical and psychosocial features among persons with schizophrenia: A mini review. Front Psychiatry 2021; 12: 789179.
http://dx.doi.org/10.3389/fpsyt.2021.789179 PMID: 35002807
[85] Ballester PL, Suh JS, Ho NCW, *et al*. Gray matter volume drives the brain age gap in schizophrenia: A SHAP study. Schizophrenia 2023; 9(1): 3.
http://dx.doi.org/10.1038/s41537-022-00330-z PMID: 36624107
[86] Baiano M, Perlini C, Rambaldelli G, *et al*. Decreased entorhinal cortex volumes in schizophrenia. Schizophr Res 2008; 102(1-3): 171-80.
http://dx.doi.org/10.1016/j.schres.2007.11.035 PMID: 18248959
[87] Wen J. Nine neuroimaging-AI endophenotypes unravel disease heterogeneity and partial overlap across four brain disorders: A dimensional neuroanatomical representation. medRxiv 2024.
[88] du Plessis S, Chand GB, Erus G, *et al*. Two neuroanatomical signatures in schizophrenia: expression strengths over the first 2 years of treatment and their relationships to neurodevelopmental compromise and antipsychotic treatment. Schizophr Bull 2023; 49(4): 1067-77.
http://dx.doi.org/10.1093/schbul/sbad040 PMID: 37043772
[89] Dwyer DB, Chand GB, Pigoni A, *et al*. Psychosis brain subtypes validated in first-episode cohorts and related to illness remission: Results from the PHENOM consortium. Mol Psychiatry 2023; 28(5): 2008-17.
http://dx.doi.org/10.1038/s41380-023-02069-0 PMID: 37147389
[90] Hwang G, Wen J, Sotardi S, *et al*. Assessment of neuroanatomical endophenotypes of autism spectrum disorder and association with characteristics of individuals with schizophrenia and the general population. JAMA Psychiatry 2023; 80(5): 498-507.
http://dx.doi.org/10.1001/jamapsychiatry.2023.0409 PMID: 37017948
[91] Wen J, Varol E, Sotiras A, *et al*. Multi-scale semi-supervised clustering of brain images: Deriving disease subtypes. Med Image Anal 2022; 75: 102304.
http://dx.doi.org/10.1016/j.media.2021.102304 PMID: 34818611